TISSUE ENGINEERING: Part A
Volume 27, Numbers 19 and 20, 2021

DOI: 10.1089/ten.tea.2020.0269

termis
Tissue Engineering
& Regenerative Medicine
International Society

ORIGINAL ARTICLE

Tissues with Patterned Vessels or Protein Release Induce Vascular Chemotaxis in an *In Vitro* Platform

Rajeev J. Kant, BS, Colette F. Bare, ScB, and Kareen L.K. Coulombe, PhD

Engineered tissues designed for translational applications in regenerative medicine require vascular networks to deliver oxygen and nutrients rapidly to the implanted cells. A limiting factor of *in vivo* translation is the rapid and successful inosculation, or connection, of host and implanted vascular networks and subsequent perfusion of the implant. An approach gaining favor in vascular tissue engineering is to provide instructive cues from the engineered tissue to enhance host vascular penetration and connection with the implant. Here, we use a novel *in vitro* platform based on the aortic ring assay to evaluate the impact of patterned, endothelialized vessels or growth factor release from engineered constructs on preinosculative vascular cell outgrowth from surrogate host tissue in a controlled, defined environment, and introduce robust tools for evaluating vascular morphogenesis and chemotaxis. We demonstrate the creation of engineered vessels at the arteriole scale, which develop basement membrane, exhibit tight junctions, and actively sprout into the surrounding bulk hydrogel. Vessel-containing constructs are co-cultured adjacent to rodent aortic rings, and the resulting heterocellular outgrowth is quantified. Cells originating from the aortic ring migrate preferentially toward constructs containing engineered vessels with 1.5-fold faster outgrowth kinetics, 2.5-fold increased cellular density, and 1.6-fold greater network formation versus control (no endothelial cells and growth factor-reduced culture medium). Growth factor release from constructs with nonendothelialized channels and in reduced factor medium equivalently stimulates sustained vascular outgrowth distance, cellular density, and network formation, akin to engineered vessels in endothelial growth medium 2 (EGM-2) medium. In conclusion, we show that three-dimensional endothelialized patterned vessels or growth factor release stimulate a robust, host-derived vascular cell chemotactic response at early time points critical for instructive angiogenic cues. Further, we developed robust, unbiased tools to quantify metrics of vascular morphogenesis and preinosculative heterocellular outgrowth from rat aortic rings and demonstrated the utility of our complex, controlled environment, heterocellular *in vitro* platform.

Keywords: tissue engineering, patterned vessels, inosculation, aortic ring, growth factor release, chemotaxis

Impact Statement

Using a novel *in vitro* platform, we show that engineered constructs with patterned vessels or angiogenic growth factor release, two methods of instructing host revascularization responses, equivalently improve early host-derived vascular outgrowth. Our platform leverages the aortic ring assay in a tissue engineering context to study preinosculative vascular cell chemotaxis from surrogate host vascular cells in response to paracrine cues from co-cultured engineered tissues using robust, open-source quantification tools. Our accessible and flexible platform enables translationally focused studies in revascularization using implantable therapeutics containing prepatterned vessels with greater environmental control than *in vivo* studies to advance vascular tissue engineering.

Introduction

A MAJOR FOCUS in tissue engineering is the creation of implantable, cellularized therapeutics that replace or augment damaged tissue. In considering the scalability of engineered constructs for clinical translation, vascularization becomes a crucial design criterion due to oxygen diffusion limits of 100–200 μm[1–3] in thick, cellularized tissue. Vascularization is particularly important in applications such as cardiac, skin, bone, liver, and pancreatic tissue

Center for Biomedical Engineering, School of Engineering, Brown University, Providence, Rhode Island, USA.

engineering that necessitate dense and hierarchically organized tissues, and thus require efficient convection of oxygen and nutrients via a robust vascular transport system.[4,5] Such tissues fabricated without vasculature and thicker than oxygen diffusion limits can suffer hypoxia and form necrotic cores.[3,6] Providing adequate conduits for the convection of oxygen and nutrients is necessary for the survival and function of implanted tissues both before and after implantation.[7–9]

Engineering vasculature within tissues *in vitro* can be achieved by using many different techniques, but it primarily involves combinatorial manipulation of physical cues (e.g., co-culture vessel stabilization,[8] fabricated geometries,[9–11] biomaterials,[2,12,13] or three-dimensional [3D] bioprinting[14,15]) and chemical cues (e.g., peptide[16] and growth factor treatment/release,[17] or co-culture paracrine signaling[8,18]) to orchestrate vessel formation.[6,19] Prevascularizing a patch before implantation has demonstrated perfusion of the implanted networks and improved survival of the construct.[9–11] The overall mechanism by which this occurs is termed inosculation, or the connection of disparate vascular networks.[20] In this process, independent vessels recognize and sprout toward one another over tens to hundreds of microns, anastomose, and remodel to form a continuous, integrated network for blood flow.[21] Inosculation can enable rapid perfusion to implanted tissues within 1–6 days after implantation,[11,22–24] which has implications for the survival, engraftment, and function of the implant.

Despite the great need for rapid vessel perfusion on implantation, preinoculative dynamics of endothelial and vascular stromal cells are not well understood. Primary literature in this area focuses on *in vitro* monolayer-based or microfluidic models that do not sufficiently recreate the complex environment and stimuli of angiogenesis at larger scales with engineered tissues,[24–27] or *in vivo* experiments that report intra-patch vessel structures or perfusion at terminal endpoints.[9,11,23,28] Thus, there is a need to examine signaling and migration patterns between host and engineered tissues before inosculation at intermediate scales in terms of time and complexity. Further, several cellular populations and microenvironmental cues engage in the inosculation process from both the host and implanted tissue and understanding how these cues drive this process is necessary to engineer an adaptive and timely vascularization response on tissue implantation.

Utilizing animal-derived tissue provides a compromise between the simplicity of *in vitro* systems and complexity of *in vivo* models[6,27,29–32] and is often used to study vascularization mechanisms, often by treatment with angiogenic agents or genetic alteration.[33,34] One such assay is the heterocellular aortic ring assay, which examines microvessel sprouting in a matrix protein (historically Matrigel) from sectioned rodent aortas stimulated primarily by VEGF, bFGF, and/or fetal bovine serum (FBS) over a 7–14 day period.[27,32] The primary outputs of this assay are microvessel counts, histological staining of endothelial and supportive stromal cells (including smooth muscle cells, fibroblasts, pericytes, etc.), and morphological assessment in response to treatment with an agent.[17,32,35,36] The aortic ring assay provides a useful starting point from which to develop a defined, robust platform for bridging studies in vascularization between *in vitro* and *in vivo* research.

In the present study, we describe and evaluate our *in vitro* platform for examining preinosculative vascular outgrowth from aortic rings in response to vascularization cues from engineered constructs in a defined and controlled environment by using a novel adaptation of the aortic ring assay. We report the global and regional migratory responses of outgrowing vascular cells adjacent to constructs containing engineered vessels and evaluate responses to physical, cellular, and chemical effectors of migration and angiogenesis by using unbiased automated analyses (in MATLAB and available online). Our data demonstrate that preinosculative outgrowth from aortic rings is sensitive to vascular stimuli and co-culture with engineered constructs, and that endothelialized vessels or growth factor release similarly prompt early vascular morphogenesis, sustained vascular outgrowth, cellular density, and cohesive network formation. We show that this platform is useful for investigation of preinoculative vascular communication and signaling between surrogate host and engineered tissues.

Methods

Sacrificial alginate fiber fabrication and construct gel casting

Alginate fibers were fabricated by using a wet spinning process. Briefly, 1% w/w sodium alginate (MilliporeSigma) solution was extruded through a 30G needle by using a syringe pump at 50 μL/s into a cross-linking bath of 100 mM calcium chloride (Acros Organics). Wet fibers were collected and dried on a mandrel (Supplementary Fig. S1).

Custom polydimethylsiloxane (PDMS) molds were fabricated as previously described.[37] Briefly, vector-based design templates were created in Adobe Illustrator (Adobe, Inc.) and etched into a 1/4" acrylic sheet by using a Universal Laser Systems 6.75 Laser Cutter (Universal Laser Systems, Brown Design Workshop). Sylgard 184 (Dow) was cast on the acrylic master and cured overnight, creating an autoclavable PDMS mold for use in sterile tissue culture (Fig. 1A). Dried sections of alginate fibers were embedded between the walls of autoclaved molds by using a 23G needle. A temporary PDMS gate was placed to prevent collagen from spilling into the ring area, and a 2 mg/mL type-1 collagen solution (Advanced BioMatrix) was then cast in the construct region. The plate was incubated at 37°C and 5% CO_2 for 30 min; then, the construct gel was immersed in phosphate-buffered saline (PBS; Gibco).

Channel patency was established by treating the construct gels with chelation media containing 1 mM sodium citrate (Fisher Scientific) in PBS for 10 min on an orbital shaker to un-crosslink the calcium alginate, and patency was confirmed by perfusion of fluorescent FluoSpheres (Fisher Scientific) or PBS (Supplementary Movie S1). To create growth factor-loaded construct gels, 10 ng/mL VEGF and 10 ng/mL bFGF were mixed into the collagen solution before casting, and chelation media contained VEGF and bFGF as well to ameliorate early burst release before ring placement. Construct gels were typically fabricated 2 days before aortic ring placement, except for growth factor releasing constructs that were created the day of ring placement.

Endothelial cell culture

Human umbilical cord endothelial cells (HUVECs; Lonza) were cultured on 0.1% gelatin- coated (MilliporeSigma)

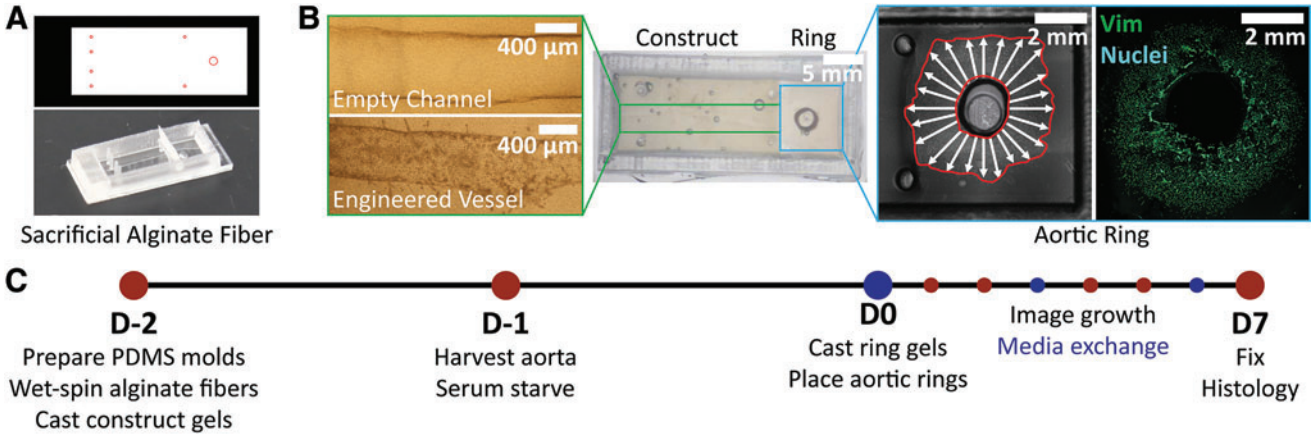

D

Media	EGM-2	EGM-2	RF EGM-2	RF EGM-2	RF EGM-2
Channel	Endothelialized	Empty	Endothelialized	Empty	Empty
Factor Release	None	None	None	None	VEGF, bFGF
Condition	+ EC	- EC	+ EC_R	- EC_R	- EC_{RG}

FIG. 1. Mold and experimental design. **(A)** Adobe Illustrator design file and corresponding PDMS mold embedded with sacrificial alginate fibers to pattern **(B)** empty channels (*top*) and engineered vessels (*bottom*; 4× magnification) within construct gels and co-culture next to outgrowing aortic rings (10× magnification). **(C)** Experimental preparation and timeline indicating media exchange. **(D)** Experimental conditions tested, denoted as engineered vessels (+ EC) or empty channels (− EC) cultured in EGM-2 or RF EGM-2 media (± EC_R), and constructs with empty channels but loaded with growth factors in RF EGM-2 (− EC_{RG}). EGM-2, endothelial growth medium 2; PDMS, polydimethylsiloxane; RF EGM-2, reduced factor medium (complete EGM-2 without VEGF and bFGF). Color images are available online.

10 cm^2 tissue culture plates (Fisher Scientific) in endothelial growth medium 2 (EGM-2; Lonza) with media exchange every day. Cells were passaged every 4–5 days at 75% confluency by enzymatic dispersion with 0.05% trypsin (Life Technologies) in versene (0.5 mM EDTA [MilliporeSigma] and 1.1 mM D-glucose [MilliporeSigma] in PBS). Cells between passages 2 and 7 were used in experiments.

Engineered vessel formation

Patent channels in constructs were seeded with 3.75× 10^7 cells/mL of HUVECs through the channel opening adjacent to the aortic ring and incubated upside down for 45 min and then right side up for 30 min to facilitate HUVEC attachment along the entire channel circumference. Constructs were then gently washed in PBS, changed into EGM-2 or reduced factor medium (EGM-2 without VEGF and bFGF; RF EGM-2), and gently perfused the next day to rinse out nonadherent cells.

Aortic ring harvest and placement

Aortas were harvested from male wild-type Sprague Dawley rats between 2 and 3 months of age and prepared by using standard protocols.[38] Briefly, rodents were anesthetized by using 4% isoflurane. The chest cavity was exposed by thoracotomy, and connective tissue was cut away to isolate the thoracic aorta. The excised aorta was cleaned of fat and connective tissue, sectioned into 1 mm tall rings, and finally serum-starved overnight in endothelial basal medium-2 (EBM-2; Lonza) +0.1 mg/mL penicillin-streptomycin (MilliporeSigma). The next day, the medium was aspirated, a 2 mg/mL collagen gel was cast adjacent to the construct gel in the ring area, and aortic rings were aligned on the central platform. Ring-construct setups were incubated for 30 min and then immersed in EGM-2 or RF EGM-2. All procedures were approved by the Institutional Care and Use Committee (IACUC) in Brown University (IACUC Approval No. 1702000256).

Imaging

Setups were imaged daily on a Nikon Eclipse Ti-E microscope (Nikon) with tiling capabilities. Histologically stained whole-mount tissues were imaged by using an Olympus FV3000 Confocal Microscope (Olympus, Brown University Leduc Bioimaging Facility). Whole-mount tissues were flattened between a glass slide and coverslip for tiling.

Outgrowth measurements

Outgrowth measurements were performed in ImageJ. Outgrowth area was calculated by drawing a region around outgrowing cells and subtracting it from the initial area of the ring. Outgrowth distance was measured in 15° increments around the ring, originating at the outer edge of the aortic ring for each angle. Regional measurements averaged 60° angle bins facing the construct gel (interface [IF] region) or away from the gel (remote [RM] region). Outgrowth velocity was calculated as the distance of each day's outgrowth subtracted by the previous day's outgrowth at each angle increment. A MATLAB (MathWorks) script was written to generate polar plots with error bars and extract centroid shift data.

Model protein release

The rate of growth factor release from collagen gels preloaded with protein was extrapolated based on bovine serum albumin (BSA) release using the bicinchoninic acid (BCA) assay. Due to the more negative charge of BSA compared with growth factors VEGF and bFGF at physiological pH and the charge interactions retaining the protein governed by negatively charged collagen, the release profile of BSA may overestimate the release kinetics. Briefly, 50 μg/mL BSA was loaded into collagen gels and cultured for 7 days in PBS +0.02% sodium azide following an identical media exchange schedule as experiments with aortic rings. Each day, 600 μL of media was removed and replaced with fresh PBS, and the aliquot was frozen. At the end of the 7 days, all media aliquots were thawed and analyzed for BSA content on a Cytation 3 Cell Imaging Multi-Mode Reader (BioTek). Values were normalized relative to cumulative release on the last day.

Immunohistochemistry

Setups were fixed in 4% paraformaldehyde (MilliporeSigma) for 15 min at room temperature, then washed with PBS, and finally stored at 4°C in the short term. Whole-mount histology was performed for most samples to preserve spatial information. Setups were blocked with 1% BSA (MilliporeSigma) in PBS for 2 h followed by overnight incubation with primary antibody in fresh blocking buffer and 0.1% Triton-X (MilliporeSigma). The next day, the setups underwent two 2-h washes in PBS, blocking for 2 h, and finally secondary antibody treatment overnight in PBS +1% BSA. On the third day, setups were treated with bisbenzimide H-33342 trihydrochloride (Hoechst; MilliporeSigma) in PBS for 15 min, three 1-h washes, and finally stored in PBS at 4°C until they were imaged. All incubation and wash steps for whole-mount histology were performed on an orbital shaker at room temperature. Some engineered vessels were fixed, processed into frozen blocks, and sectioned on an Avantik QS12 cryostat (Brown University Molecular Pharmacology, Physiology, and Biotechnology). Histology then proceeded as described earlier. Primary and secondary antibodies used are provided in Table 1.

Image analyses

Histological analysis was performed in MATLAB by first defining regions of interest (ROIs) within inner and outer subdivisions of the IF and RM regions. Within ROIs, Hoechst stains were evaluated by watershed segmentation to obtain nuclear counts. Nearest-neighbor analysis was performed by implementing a pixel search algorithm to find particles within 20 μm of each other. Nuclear orientation was determined by excluding uniform nuclei based on aspect ratio and normalizing each particle's major axis orientation by the angle of outgrowth from the ring. Network area measurements were taken from vimentin stains and separated into isolated cell or network masks. All MATLAB codes are hosted online and free to download and use via the Harvard Dataverse.

Statistical analysis

Statistics were calculated by using one-way or two-way repeated-measures analysis of variance as appropriate, followed by the Tukey-Kramer method of *post hoc* analysis with p-values <0.05 being considered statistically significant. All analysis was performed in Prism 8 (GraphPad). Sample size denoted as n refers to individual aortic rings. Each condition contains between three and eight biological replicates (aortas from distinct animals) from which between two and four aortic rings were quantified per group.

Table 1. List of Antibodies Used for Immunohistochemistry

Antibody/fluorophore	*Dilution*	*Catalog No.; company*
Mouse monoclonal anti-vimentin	1:200	V6630-100 UL; MilliporeSigma
Mouse monoclonal anti-collagen IV	1:100	SAB4200709-100 UL; MilliporeSigma
Rabbit polyclonal anti-human VE-cadherin	1:50	36-190-0; Fisher
Bisbenzimide H 33342 trihydrochloride (Hoechst)	1.5 μg/mL	B2261-100MG; MilliporeSigma
Goat anti-mouse Alexa Fluor 488	1:400	A-11001; Invitrogen
Goat anti-rabbit Alexa Fluor 594	1:400	A-11005; Invitrogen
Griffonia Simplicifolia Isolectin B4, Dylight 594-labeled	1:400	DL-1207-.5; Vector Labs

Experiment

Culture mold design enables co-culture of aortic rings with constructs containing engineered vessels

Our PDMS mold-making process as previously published for *in vitro* and *in vivo* implant fabrication[17] was adapted to enable the co-culture of rodent aortic rings next to a construct.[37] For this design, cylindrical posts were arranged in the construct area to anchor the gel in place during culture (Fig. 1A). A larger cylindrical platform centrally located in the ring region enabled precise placement of aortic rings at the same distance (2 mm) from the construct gel without contacting the ring intima. The overall mold size was optimized to accommodate imaging of vascular cell outgrowth over 7 days and fit a construct approximating the size appropriate for subcutaneous or epicardial implantation in rats (Fig. 1B).

Setups were imaged daily, fed every third day, and fixed on day 7 for immunohistochemical staining and analysis (Fig. 1C). Our experimental conditions were selected to elucidate specific contributions of endothelial cells and growth factors to vascular outgrowth, and thus inform *in vivo* implant design choices (Fig. 1D). Construct gels contained either nonendothelialized channels (− EC) or engineered vessels (+ EC) and were fed with either EGM-2 or RF EGM-2 (denoted as ± EC_R). Lastly, to determine how spatiotemporal presentation of growth factors affected outgrowth response in comparison to stagnant media-solubilized presentation, we loaded 10 ng/mL VEGF and bFGF into construct gels without HUVECs and co-cultured those with aortic rings in RF EGM-2 (− EC_{RG}).

Endothelialized channels form functional engineered vasculature and exhibit sprouting

Alginate fibers were fabricated by using a wet spinning technique (Supplementary Fig. S1) and utilized as sacrificial templates to pattern perfusable, arteriole-scale channels in construct gels with an average diameter of 461.5 ± 15.6 μm (Supplementary Movie S1). Engineered vessels were established by seeding HUVECs into channels, which proliferated to fill the circumference as confirmed by CD-31 staining (Fig. 2A and Supplementary Fig. S2A). *En face* sections of the vascular wall showed a confluent monolayer with tight junctions marked by VE-cadherin and deposition of the basement membrane protein collagen IV, indicative of appropriate vascular structure (Fig. 2B). Engineered vessels cultured in RF EGM-2 were similarly able to form fully confluent walls with VE-cadherin expression and maintain patency, although delamination from the collagen gel wall occurred to varying degrees in 88% of engineered vessels by later time points (Fig. 2C, inset, dashed lines). In contrast, engineered vessels cultured in EGM-2 medium did not exhibit any delamination. For all experiments, HUVECs were seeded in channels 2 days before embedding aortic rings (denoted as day -2) to allow for infill of the vessel wall.

Diameter measurements over the study revealed a reduction to about 80% of initial diameter independent of culture media (79.1% ± 2.37% and 78.0% ± 2.82% for + EC and + EC_R groups, respectively) due to HUVEC remodeling of the construct gel matrix (Fig. 2D). Nonendothelialized channels exhibited a slight increase in diameter (108.2% ± 1.82%), likely due to sagging of the channel into an ellipsoid cross-section during the experiment.

Vascular sprouting was evident from engineered vessels in both media compositions (Fig. 2E–H). Engineered vessels cultured in EGM-2 demonstrated peak sprouting at 3–4 days after seeding followed by divergence into two distinct morphologies, with 57% of samples developing dense vascular plexuses with active tip-stalk sprouting throughout the experiment (Fig. 2A, E, inset, white arrows) and the rest exhibiting transient sprouting followed by regression and quiescence of the main vessel (Supplementary Fig. S2B). Live/dead staining of quiescent vessels at day 7 showed that the main vessel maintained full coverage with a few apoptotic cells, attributed to either sprout regression or death during the seeding process (Supplementary Fig. S2C). In contrast, engineered vessels cultured in RF EGM-2 had significantly fewer sprouts with a peak at day -1 followed by quick regression of all sprouts (Fig. 2F, inset).

Sprouting morphology varied between groups, with simple spur sprouts being the dominant morphology across + EC and + EC_R occurring either transiently or persistently in 92% and 83% of engineered vessels, respectively, during culture (Supplementary Fig. S2D, E). Split sprouts (multiple spurs with a common root) occurred in 69% of + EC vessels; however, it occurred in only 17% of + EC_R vessels. Sprouts from + EC vessels additionally exhibited branches (spurs with a sprouting node above the root; 77%), loops (distinct spurs that form a linked vessel; 69%), and complex sprouts (combinations of the described morphologies including plexuses; 46%). Together, our data show that perfusable engineered vessels

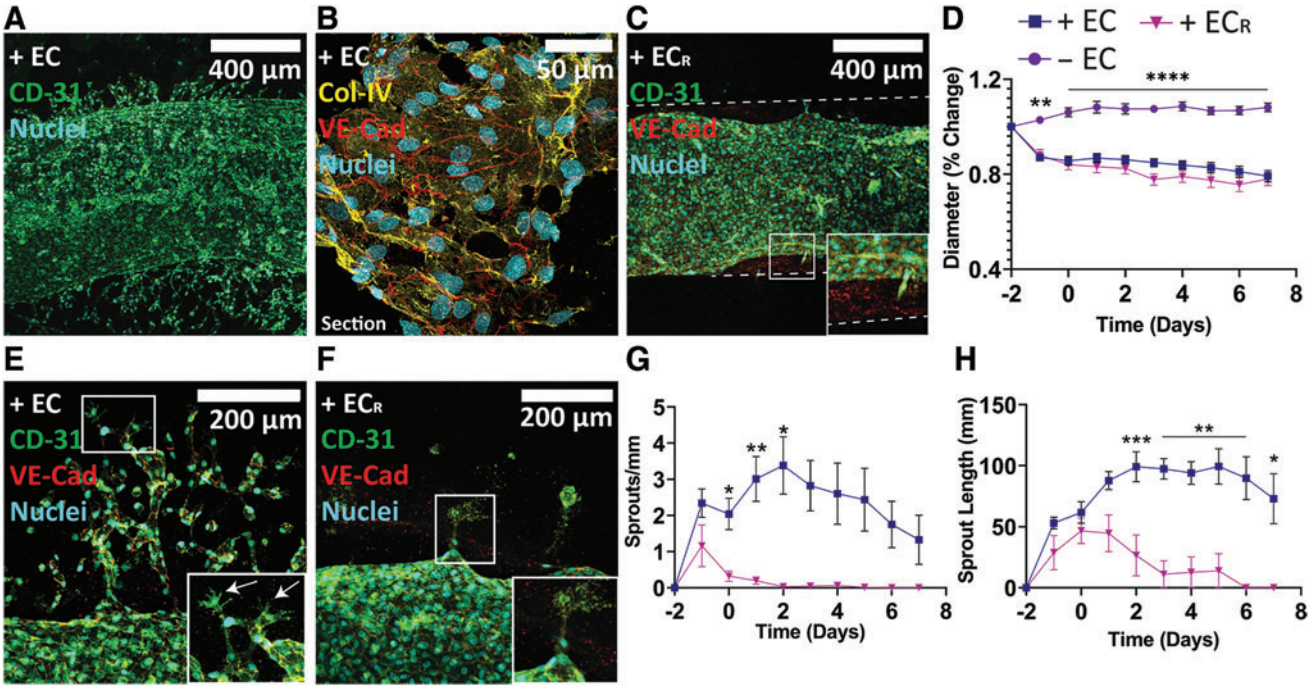

FIG. 2. Endothelialization of empty channels. **(A)** Whole-mount histology of engineered vessel in complete media (10× magnification) and **(B)** section view of the vessel wall (60× magnification). **(C)** Engineered vessel cultured in RF EGM-2 (10× magnification). *Inset* shows partial delamination of vessel from vessel wall (*dashed lines*). **(D)** Quantification of engineered vessel diameter. **(E)** Sprouting behavior in engineered vessels in EGM-2 (20× magnification). *Inset* shows tip-stalk phenotype of sprouts, with *arrows* indicating tip cells. **(F)** Sprout regression in RF EGM-2 (20× magnification). **(G, H)** Quantification of sprouting behavior from engineered vessels. + EC ($n = 14$), − EC ($n = 11$), + EC_R ($n = 6$). *$p < 0.05$, **$p < 0.01$, ***$p < 0.001$, ****$p < 0.0001$. Color images are available online.

formed in construct gels demonstrate structural properties of native vasculature and actively sprout into the construct bulk gel in the presence of soluble pro-angiogenic growth factors.

Global vascular outgrowth is natively influenced by physical cues but overridden by paracrine or chemical signaling

After placement of the aortic rings adjacent to construct gels, daily phase-contrast images showed consistent outgrowth in all directions relative to the outside edge of the ring (Fig. 3A). Experiments were performed without engineered vessel perfusion to study a static, nonperfused tissue microenvironment as would occur immediately on implantation if used for translational *in vivo* studies where surgical vascular anastomosis is not used. Outgrowth measurements were taken in 15° increments around the rings each day, from which we found significant differences between + EC and − EC groups at day 3 (Supplementary Fig. S3A). Area quantification revealed improved outgrowth for the $-EC_{RG}$ and $+EC_R$ groups compared with the − EC group by day 5 and a significant increase in area between the + EC and − EC groups by day 6 (Supplementary Fig. S3B).

By visualizing the data by using polar plots, we noted nonuniform outgrowth in aortic ring setups that appeared to be dependent on the presence of engineered vessels and growth factors solubilized in media or locally released (Fig. 3B). We quantified this bias by calculating the average horizontal shift in the centroid of outgrowth over the course of the experiment (Fig. 3C) and observed an apparent rightward shift in cellular migration (away from construct gels with nonendothelialized channels) most severe in the $-EC_R$ group, indicating a rightward bias in outgrowth that may be due to collagen fiber orientation during gelation, mechanical differences due to imperfect coupling of the construct and ring gels, or overall mold geometry. However, this effect was ameliorated in the − EC group and entirely reversed to a left-ward bias in migration toward engineered vessels in both media compositions as well as growth-factor loaded construct gels in RF EGM-2, showing a strong outgrowth bias in response to growth factors and engineered vessels.

In examining population velocity per day, the + EC group showed a significant increase in migration velocity at day 2 in comparison to all groups except $-EC_{RG}$, which itself almost reached significance relative to $-EC_R$ ($p=0.084$) (Fig. 3D and Supplementary Fig. S3D). On day 3, we found increased outgrowth velocity for both + EC and $-EC_{RG}$ relative to − EC. At later time points, the average velocity values per day slowly decreased with no significant differences between groups. Lastly, we used the BCA assay to

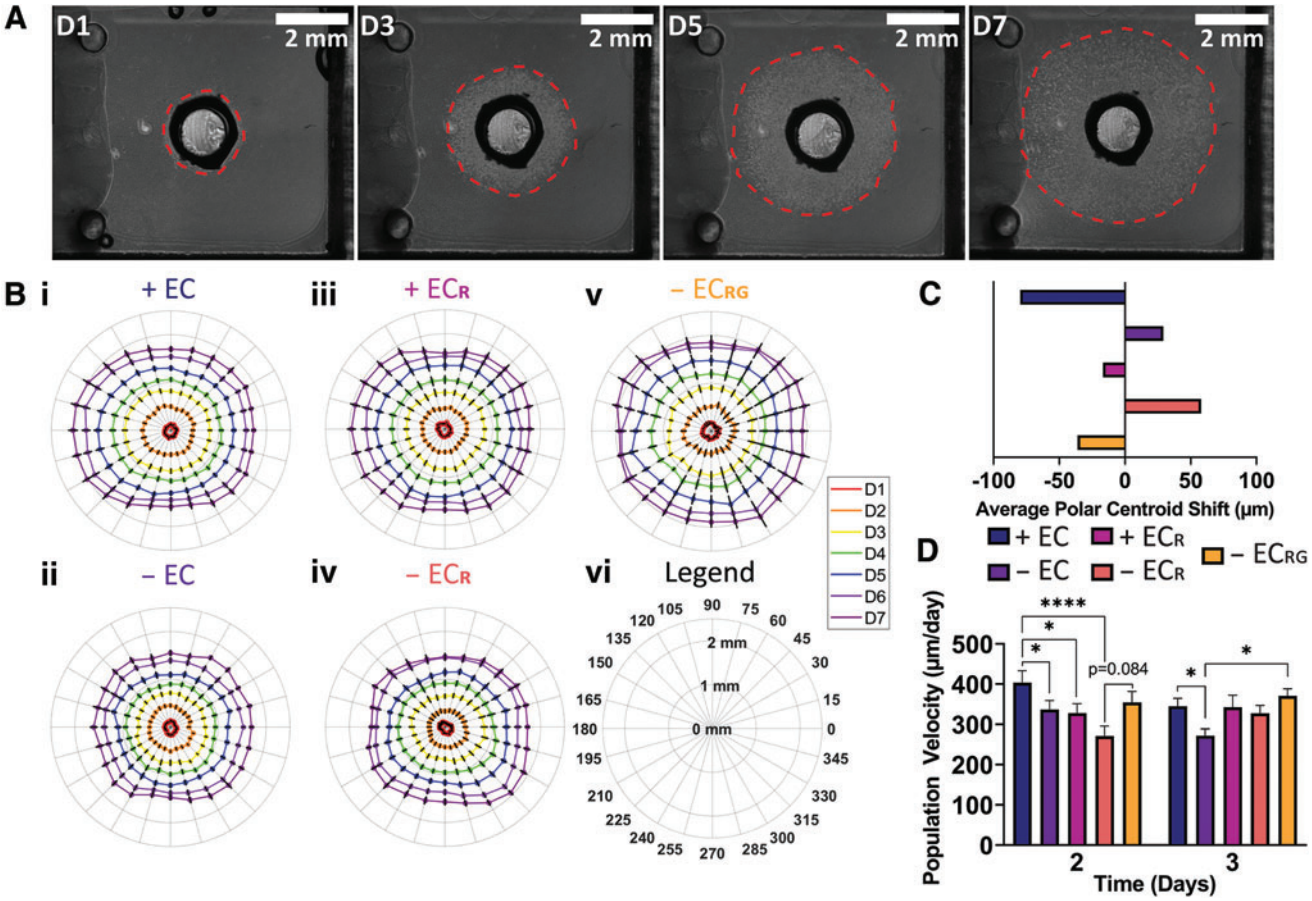

FIG. 3. Population outgrowth from aorta-derived cells. **(A)** Aortic outgrowth progression (4×magnification) and **(B)** polar plots of vascular outgrowth for each condition **(i–vi)**. **(C)** Average *left-right* centroid shift in population outgrowth for each group. **(D)** Average population velocity of aortic outgrowth at days 2 and 3. + EC ($n=17$), − EC ($n=15$), $+EC_R$ ($n=11$), $-EC_R$ ($n=11$), $-EC_{RG}$ ($n=8$). $^*p<0.05$ and $^{****}p<0.0001$. Color images are available online.

quantify release from collagen gels, which revealed significant burst release within the first day followed by lower, sustained release over the next 3 days (Supplementary Fig. S3E). These data suggest that a combination of physical, cellular, and chemical signals bias vascular cell outgrowth distance and velocity. The culture design appears to impart a physical cue that influences migration away from the engineered construct, but this directional growth is overridden by endothelial cell paracrine signaling from engineered vessels. Further, angiogenic growth factor release from gels provides a similarly strong and sustained stimulus as compared with endothelial cell paracrine signaling, despite early burst release and in otherwise reduced factor conditions, for improving and biasing overall vascular cell outgrowth.

Vascular outgrowth distance is increased toward constructs by paracrine signaling from endothelial cells and growth factors

To further investigate specific biases in outgrowth direction, we binned the outgrowth measurements into 60° intervals toward or away from the construct gel, referred to as the IF and RM regions, respectively (Fig. 4A). Using this methodology, we were able to see significant increases in outgrowth distance in the IF region as early as day 2 between both + EC and − EC_{RG} relative to − EC_R that were sustained throughout the rest of the experiment. (Fig. 4B, C). At day 3, we found additional significant increases for both + EC and − EC_{RG} relative to − EC that were similarly sustained. By day 7, the + EC and − EC_{RG} groups reached an average IF outgrowth distance of 2076.32 ± 88.04 μm and 1966.57 ± 62.67 μm, respectively, whereas the − EC and − EC_R reached IF outgrowth values of only 1607.67 ± 83.35 μm and 1632.48 ± 50.67 μm. We were unable to find significant differences for the + EC_R group (1935.45 ± 102.12 μm) relative to − EC ($p = 0.13$) or − EC_R ($p = 0.11$). In comparing IF and RM outgrowth at day 7, we found a significant difference only within the + EC group (Fig. 4F, + signs). Further, we examined regional velocity at early (days 1–4) and late (days 4–7) time points and found significantly increased early migration velocity in the IF region for + EC and − EC_{RG} groups relative to − EC, although neither reached significance when compared with − EC_R ($p = 0.12$ and $p = 0.20$, respectively) (Fig. 4D). In stark contrast, we did not find any significant differences between groups in the RM region in either outgrowth distance or velocity (Fig. 4E–G).

We further examined chemical effectors of outgrowth by supplementing some + EC setups with additional FBS up to 10% (+ EC_{10FBS}) and saw greater increases in population and regional outgrowth, area, and velocity in comparison to + EC, attributed to the greatest increases in the RM region (Supplementary Fig. S4A–E). Setups supplemented with FBS also experienced greater compaction, which affected outgrowth measurement accuracy of some samples, and day 7 measurements were omitted from analysis due to hypercompaction.

Together, these data show that endothelial cells and growth factors bias vascular cell outgrowth and morphogenesis. Paracrine signaling from engineered vessels in EGM-2 resulted in outgrowth matched only by growth factor release in RF EGM-2, which was sustained for the entire 7 days despite loaded factor burst release and media exchange. Engineered vessels in RF EGM-2 may provide an intermediate level of benefit in outgrowth but they suggest that implanted engineered vessels without growth factors do not provide as favorable a microenvironment as media tailored to endothelial cell growth. These cellular and chemical stimuli caused microenvironmental changes to influence outgrowth distance and velocity in the local IF region.

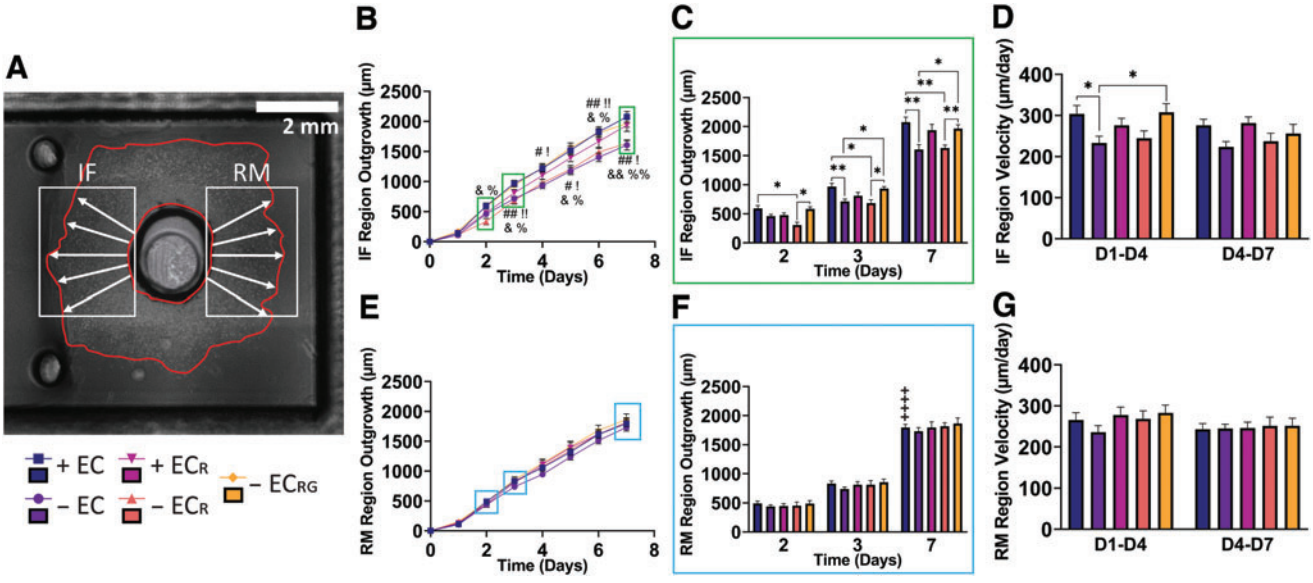

FIG. 4. Regional outgrowth analysis. **(A)** Binning methodology for IF and RM regions (4× magnification). **(B, E)** Outgrowth over time with **(C, F)** differences highlighted at days 2 and 7, and **(D, G)** regional average velocity for IF and RM regions, respectively. + EC ($n = 17$), − EC ($n = 15$), + EC_R ($n = 11$), − EC_R ($n = 11$), − EC_{RG} ($n = 8$). $^{*, \#, !, \&, \%}p < 0.05$, $^{**, \#\#, !!, \&\&, \%\%}p < 0.01$, $^{***}p < 0.001$, $^{++++}p < 0.0001$. $^{\#}$Significance between + EC and − EC. $^{!}$Significance between − EC_{RG} and − EC. $^{\&}$Significance between + EC and − EC_R. $^{\%}$Significance between − EC_R and − EC_{RG}. $^{+}$Significance between IF and RM regions for indicated group at day 7. IF, interface; RM, remote. Color images are available online.

Paracrine endothelial cell signaling and growth factor release improve IF region outgrowth density and cell clustering

Imaging revealed multiple layers of outgrowth that formed over time, and we noted stark differences in morphology on comparing vascular outgrowth in the IF and RM regions between groups (Supplementary Fig. S5A). The + EC and − EC groups reliably exhibited dense outgrowth relative to + EC_R and − EC_R (as demonstrated by the greater white contrast, particularly adjacent to the ring), with the least density and networking apparent in the − EC_R group. Growth factor release in the − EC_{RG} group appeared to ameliorate this, with average density between EGM-2 and RF EGM-2 groups. This pattern was upheld when considering network formation between neighboring cells (Supplementary Fig. S5A, white arrows). We additionally observed relatively greater density and networking in the IF regions of + EC, + EC_R, and − EC_{RG} groups when compared with their respective RM regions.

We thus sought to quantify the differences in density and networking observed between treatment groups through whole-mount histology at day 7 to best preserve gross morphology and orientation. Histological analysis in MATLAB was performed by defining inner and outer subregions for both IF and RM regions from which to specify ROIs (Fig. 5A). This subdivision allowed us to capture heterogeneity in cellular density at different areas within the outgrowth regions that were otherwise not as clear in whole-region analysis (Supplementary Fig. S6A–C). Nuclear density was quantified on Hoechst stains followed by nearest-neighbors analysis in a 20 μm search radius to characterize local clustering as a microenvironmental output of cell–cell interactivity relative to the macroscale-focused nuclear density metric (Fig. 5B, C). In the inner IF subregion, the + EC group had significantly higher nuclear density at 2749.65 ± 271.29 nuclei/mm^2 relative to both RF EGM-2 groups (1507.91 ± 154.90 nuclei/mm^2 and 1116.00 ± 184.23 nuclei/mm^2 for + EC_R and − EC_R, respectively). The − EC (2230.39 ± 138.80 nuclei/mm^2) and − EC_{RG} (2288.50 ± 305.71 nuclei/mm^2) groups were significantly higher compared with − EC_R, but not relative to + EC_R ($p = 0.164$ and $p = 0.202$, respectively). We also found significant decreases in nuclear count in the outer subregions for + EC (1186.03 ± 174.57 nuclei/mm), − EC (935.62 ± 120.09 nuclei/mm), and − EC_{RG} (859.52 ± 85.85 nuclei/mm) groups

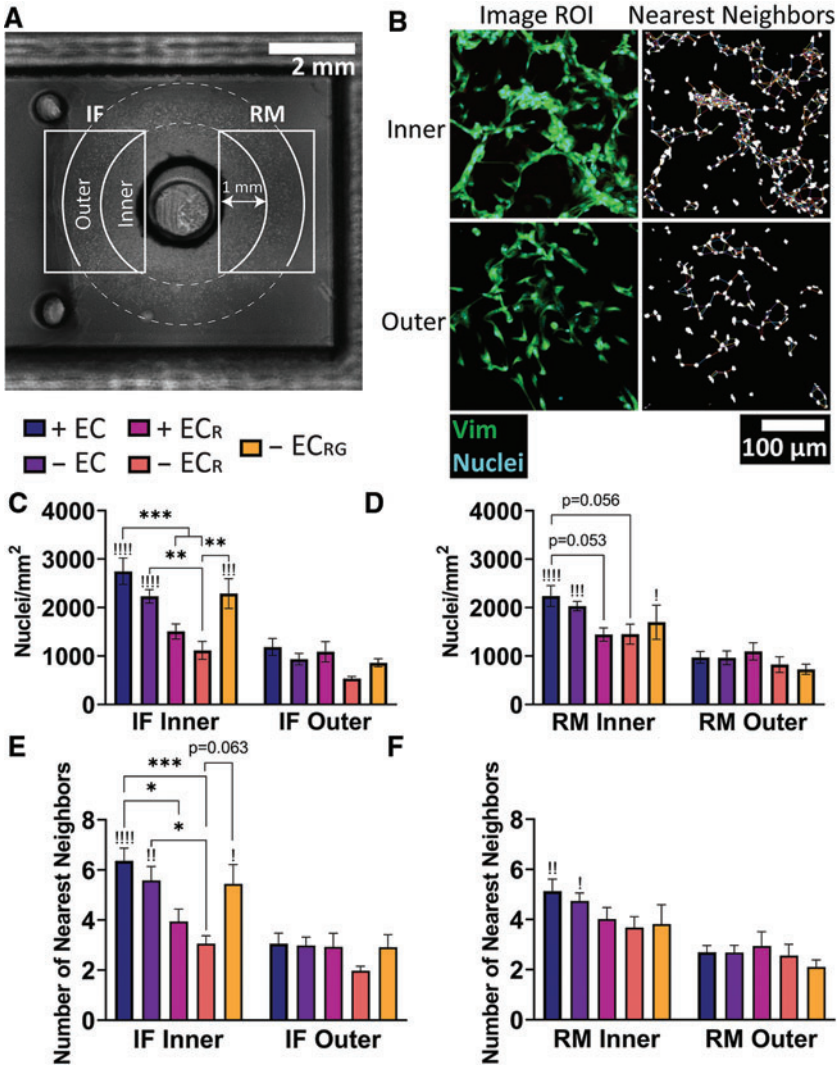

FIG. 5. Histological evaluation of outgrowth regions. **(A)** Subregion specification within IF and RM regions used for quantification (4× magnification) due to **(B)** observed differences in density and morphology in outgrowing cells (10× magnification). Quantification of **(C, D)** nuclear density and **(E, F)** nearest neighbors within 20 μm in the IF and RM regions. [!]Significance between inner and outer subregion for that condition. + EC ($n = 8$), − EC ($n = 8$), + EC_R ($n = 6$), − EC_R ($n = 6$), − EC_{RG} ($n = 5$). [*, !]$p < 0.05$, [**, !!]$p < 0.01$, [***, !!!]$p < 0.001$, [!!!!]$p < 0.0001$. [!]Significance between inner and outer subregions within that group. Color images are available online.

when compared with their inner region counterparts (indicated with exclamation points). In contrast, we found shifts in the inner RM region that did not quite reach significance between + EC (2239.85 ± 213.96 nuclei/mm) and both + EC_R (1444.40 ± 138.90 nuclei/mm, $p = 0.053$) and − EC_R (1451.17 ± 205.70 nuclei/mm, $p = 0.056$) groups, and significant differences in inner-outer subregion density for the + EC, − EC, and − EC_{RG} groups (Fig. 5D).

Nearest-neighbors analysis revealed greater clustering in the + EC group (6.36 ± 0.51 neighbors) relative to + EC_R (3.95 ± 0.49 neighbors) and − EC_R (3.06 ± 0.31 neighbors) groups (Fig. 5E). The − EC group (5.59 ± 0.55 neighbors) was significant only compared with − EC_R ($p = 0.306$ relative to + EC_R). − EC_{RG} (5.44 ± 0.78 neighbors) did not reach significance relative to + EC_R ($p = 0.600$) but was almost significant when compared with − EC_R ($p = 0.063$), suggesting a possible contribution of short-term factor release to clustering in depleted factor conditions. Clustering in the IF outer regions dropped significantly for + EC (3.06 ± 0.42 neighbors), − EC (2.99 ± 0.33 neighbors), and − EC_{RG} (2.92 ± 0.50 neighbors) groups, and by comparison, only decreased appreciably between the RM subregions for the + EC (5.13 ± 2.69 neighbors to 2.69 ± 0.27 neighbors) and − EC (4.74 ± 2.68 neighbors to 2.68 ± 0.29 neighbors) groups (Fig. 5F). In quantifying numbers of cells without neighbors in the 20 μm search radius, we found significant increases in the IF region between − EC_R and both + EC and − EC, but not + EC_R ($p = 0.183$) or − EC_{RG} ($p = 0.205$) groups (Supplementary Fig. S6D). We additionally examined nuclear orientation of segmented particles within the inner and outer regions of each group (Supplementary Fig. S6E.i–v). Histogram plots showed a relatively flat distribution of cell angles, although the RF EGM-2 groups appeared to have greater variability in distribution at extreme angles.

These results show that engineered vessels and growth factor conditions drive differences in regional and subregional nuclear density and clustering. Growth factors had a dominant effect on these parameters when presented in media with engineered vessels or if factor release was controlled, whereas engineered vessels in RF EGM-2 were unable to significantly improve outgrowth. Release of growth factors improved outgrowth density and clustering in a manner comparable to groups in EGM-2 media without endothelial cells and was most pronounced in the IF region, indicating regional differences in the microenvironment closer to the construct.

Network morphology shows cohesive structures with locally released growth factors or endothelial cells in a growth factor-rich environment

Lastly, we sought to quantify population-level network formation in the heterocellular outgrowth as it is a vital component of preinosculative migration. Histological staining with isolectin B4 (IB4) confirmed the presence of outgrowing endothelial cells but did not quite capture all outgrowing cells (Supplementary Fig. S7A). In contrast, staining for the intermediate filament protein vimentin (present in a variety of cell types including endothelial cells,[39] pericytes,[40] and smooth muscle cells[41,42]) showed wide expression in outgrowing cells and was thus chosen for population-level quantification. Vimentin stains in each defined subregion were analyzed by applying threshold masks to distinguish networks and isolated cells based on size (Fig. 6A). In comparing our original ROIs and network masks, we noted differing morphologies that corresponded to either true network-like structures associated with multiple nuclei, cell–cell adhesions, and tube-like structures (Fig. 6A, white

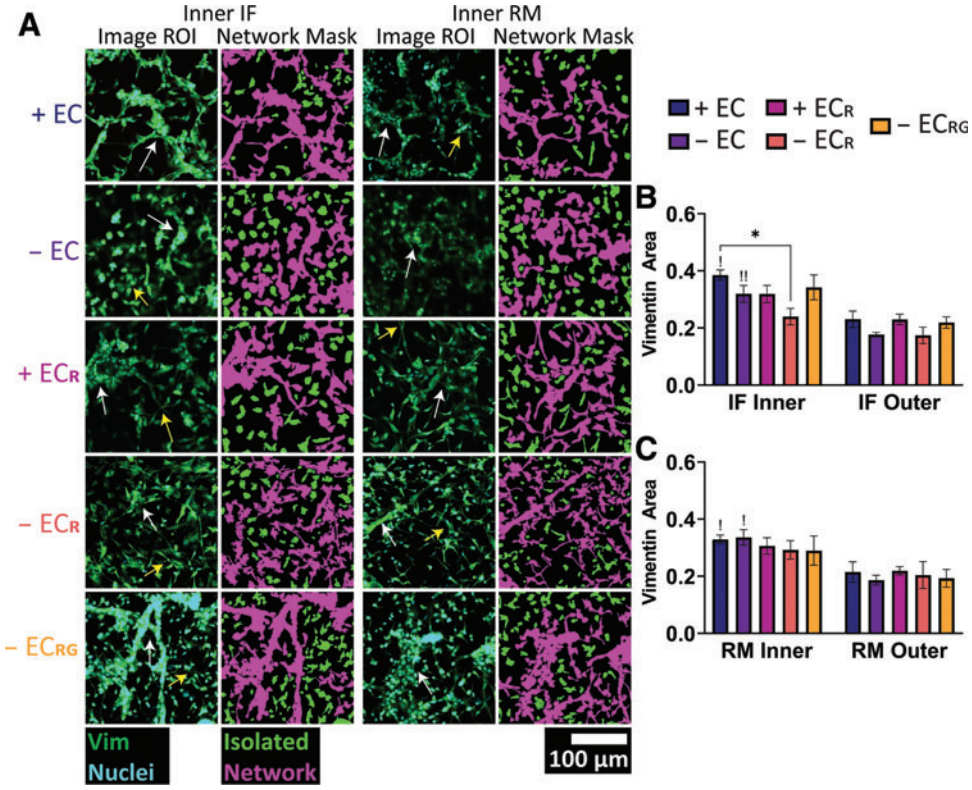

FIG. 6. Vascular histomorphological evaluation in outgrowth regions. **(A)** Representative histological stains in the inner IF and RM regions for each group and corresponding isolated cell and network masks (10× magnification). *White arrows* indicate true networks, and *yellow arrows* indicate overlapping cells. Cell area as quantified by vimentin stains in the **(B)** IF and **(C)** RM regions. + EC ($n = 5$), − EC ($n = 7$), + EC_R ($n = 6$), − EC_R ($n = 6$), − EC_{RG} ($n = 5$). $^{*,\ !}p < 0.05$, $^{!!}p < 0.01$. $^{!}$Significance between inner and outer subregions within that group. Color images are available online.

arrows), or elongated cells that did not appear to robustly interact with neighboring cells or were overlapping from a different plane (Fig. 6A, yellow arrows). These true networks were most often seen in both EGM-2 groups and comparably in the $-EC_{RG}$ group. The mask of isolated cells additionally captured two distinct cell morphologies consisting of cells with elongated projections characteristic of mesenchymal cells and more compact, amoeboid-like morphologies. Isolated cells appeared most frequently in the $+EC_R$ and $-EC_R$ groups and to a relatively lesser extent in the $-EC_{RG}$ group, although the masking algorithm erroneously labeled some clusters or overlapping cells as networks.

Consequently, in quantifying average vimentin stain area, we found significant increases in vimentin area in the + EC group at $38.5\% \pm 1.8\%$ compared with $24.0\% \pm 2.9\%$ for $-EC_R$ in the inner IF region and significantly decreased area between inner and outer subregions for + EC and − EC groups in both IF and RM regions (Fig. 6B, C). Vimentin area for the $-EC_{RG}$ group ($34.2\% \pm 4.4\%$ in IF inner, $21.9\% \pm 2\%$ in IF outer, IF inner-outer $p = 0.095$) was not quite significant relative to $-EC_R$ ($p = 0.21$) and not different compared with + EC ($p = 0.98$). We were also unable to find any significant differences across sub-regions nor in our regional analysis of single-cell and network masks (Supplementary Fig. S8A–D) due to the multi-layered outgrowth observed and confirmed with high-magnification Z-stacks showing a distinct and dense primary layer of extended and networked cells, and additional upper layers of sparsely populated and increasingly compact and noninteractive cells (Supplementary Fig. S8E).

Together, these results show that vascular outgrowth is multilayered and heterocellular in nature. Network formation is most significantly impacted by paracrine signaling from engineered vessels in medium containing angiogenic factors, and removal of these cues impacts robust network interactions. Growth factors alone, whether solubilized in media or presented via localized release from the hydrogel, are similarly able to initiate early endothelial cell morphogenesis and develop a comparable amount of cohesive network formation despite the lack of endothelialized channels in the latter case. This suggests the importance of timely presentation of chemical factors and paracrine signaling from engineered vessels for preinosculative network formation, stromal cell recruitment, and chemotaxis toward engineered constructs.

Discussion

Inosculation is a crucial process in establishing blood flow to implanted, engineered tissues containing prepatterned vasculature, and thus it is imperative to understand how engineered tissues influence host-derived pro-inosculative migration and cell recruitment in a complex but controlled, heterocellular environment. In this study, we utilized our novel co-culture platform between heterocellular aortic rings and engineered constructs (Fig. 1) containing patterned, arteriole-scale engineered vessels (Fig. 2) to investigate factors beneficial for preinosculative outgrowth. Migration distance was regionally biased by engineered vessels and growth factors whether in the culture medium or locally released (Figs. 3 and 4), and both tissue-engineered approaches also improved cellular density and clustering (Fig. 5). Combined endothelial cell signaling and culture medium containing angiogenic factors best improved network formation relative to control, with growth factor release inducing comparable network formation (Fig. 6). Our novel *in vitro* co-culture platform demonstrates that preinosculative outgrowth can be spatiotemporally directed by appropriate and timely presentation of cellular or chemical cues to facilitate equivalently effective early vascular morphogenesis and chemotactic sprouting toward engineered vasculature.

Selection of an assay or system for evaluating angiogenesis and vascular morphogenesis is an important design choice based on the desired outcome and downstream goals. *In vitro* assays[27] such as the two-dimensional (2D) network formation assay or Boyden chamber can provide a highly simplified approach to characterizing basic angiogenic phenomena, and organ-on-chip systems can provide more sophisticated methods of fabricating tightly controlled systems to study specific mechanisms such as capillary perfusion[43] and interstitial flow.[25] However, these are not inherently translational systems designed to accommodate large engineered tissues, can be limited to shorter duration studies, and typically do not involve complex, dynamic, heterocellular environments. *In vivo* assays such as the arterio-venous (AV) loop[44] and dorsal skinfold chamber[45,46] provide opportunities for studying vascularization at the arteriole and capillary scales, respectively, and can be relatively controlled in comparison to subcutaneous or organ-specific implantation sites due to the isolated chambers in which an implanted tissue is cultured. However, size and throughput are limiting factors for assessing preinosculative vascular dynamics, and they do not provide the same design flexibility of the aortic ring assay. Other assays using animal derived tissues such as the chicken chorioallantoic membrane[29] or murine/leporine retina[30] assays can also provide a complex, heterocellular pro-angiogenic site with which to evaluate a therapeutic, with the latter being similar in nature to the aortic ring assay. However, the former assay utilizes an actively developing, multi-organ, and nonmammalian tissue.

Thus, we selected the aortic ring assay as an appropriately complex, mammal-based, medium throughput for the goals of the study. Previous literature has utilized the aortic ring in a co-culture environment, with the inferior vena cava of rodents to study AV anastomosis[47] and co-culture with human plaques to examine atherosclerotic-induced angiogenesis.[48] To the best of our knowledge, this study is the first to examine aortic ring co-culture with vascularized engineered constructs in a translationally relevant platform to investigate preinosculative host-implant vascular growth. In our study, we focused primarily on pertinent chemical and cellular cues driven by engineered construct composition, and their effect on surrogate host vascular morphogenesis and chemotaxis using robust quantitative tools.

The diameter of engineered vessels in our constructs was informed by published literature showing an inability of patterned microvessels <200 μm diameter to maintain geometry and perfusion after implantation, whereas larger vessel diameters promoted greater perfusion. Redd *et al.* demonstrated rapid vascularization and perfusion of cardiac patches with microfabricated 150 μm diameter vessels implanted on the relatively avascular postinfarct rat heart but were unable to confirm the maintenance of original channel geometry,[9] whereas Baranski *et al.* successfully maintained

the geometry of patterned, ~75 μm diameter endothelial cords for 14 days and were perfused in as little as 3 days after implantation on the parametrial fat pad of athymic mice.[11] Debbi *et al.* recently reported improved inosculation, perfusion, and vessel coverage of subcutaneously implanted patches with self-assembled capillaries and ~350 μm patterned vessels when compared with those with only microvasculature, but reported finding perfused vessels no larger than ~50 μm at explant.[28] These findings indicate that implant location, host tissue state, and remodeling play important roles in the maintenance of patterned vessel geometries. Further, Mirabella *et al.* showed that patterned 400 μm vessels were better able to direct collateralization and rescue perfusion in an ischemic hind limb model compared with 200 μm channels,[15] suggesting that patterned vessel diameter is a key consideration for developing vessel-patterning therapeutics and enabling oxygen and nutrient transfer to ischemic regions. Our wet spinning parameters were consequently optimized to create alginate fibers and thus channels with an initial diameter of ~450 μm before compaction by resident HUVECs. The vessels were patterned in collagen gels with dimensions suitable for future *in vivo* subcutaneous or epicardial implantation studies in rodents,[17] as well as appropriately sized for co-culture with aortic rings.

The engineered vessels exhibited sprouting into the construct gel in EGM-2 medium, often in localized regions and forming complex vascular plexuses. We hypothesize that nonuniform concave pockets in alginate fibers due to rapid cross-linking kinetics[49] and swelling could result in channel wall concavities, causing heterogenous HUVEC seeding and thus plexus formation. Conversely, uniform fibers would allow homogenous seeding and correspondingly less sprouting into the bulk. Sprout regression followed to varying degrees, as was expected in vessel sprouts with no pericytes or other supportive stromal cells.[50] The contrasting engineered vessel phenotypes observed could differentially bridge a host-implant vascular gap via a bottom-up approach of angiogenic sprout inosculation or a hierarchical top-down style of inosculation with a quiescent vessel. Studies, including Redd *et al.*[9] and Debbi *et al.*,[28] suggest there are benefits to this multi-scaled approach to implant vascularization, and our platform provides an adequately complex foundation from which host-implant vascular interactions and preinosculative migration can be pursued without many of the complications or considerations of *in vivo* experiments.[27,32,51]

Two growth factors, VEGF and bFGF, are secreted by endothelial cells and vascular stromal cells and are primary drivers of angiogenic outgrowth, necessitating careful consideration of their presence (or absence) in our study. Angiogenesis is mediated by Notch signaling upstream of VEGF activation via Dll-4 and molecularly linked Wnt signaling to enable tip cell specification and consequent stalk cell specification of surrounding endothelial cells.[52,53] This enables new sprouts to form from activated endothelial cells and undergo chemotaxis along pro-angiogenic growth factor gradients and has been demonstrated in aortic rings.[32,48] bFGF is shown to participate in angiogenesis via multiple downstream signaling cascades, including PI3K, Ras, and Src pathways.[54] Other angiogenic signaling molecules may also initiate and modulate vascular responses, such as angiopoietins, which can induce inflammatory-mediated angiogenic remodeling via the TEK pathway to generate new sprouts and recruit mural cells for stabilization.[20,55] These angiogenesis pathways are highly relevant during inosculation wherein separate vascular sprouts migrate toward each other and anastomose to form a cohesive network. However, it is not clear what pathways facilitate the recognition process preceding migration, or whether paracrine and autocrine regulatory mechanisms differentiate between independent sprouting and inosculation processes in endothelial cells, which are questions that further studies could address.

The vascular outgrowth we observed was modulated by engineered vessels and presentation of growth factors, suggesting that these cues heightened growth factor gradients to drive preinosculative directional migration. In contrast, the reduced factor culture medium composition (no exogenous VEGF and bFGF) may be more akin to an *in vivo* microenvironment with regards to readily available growth factors, likely compromising the proliferative, migrative, and tubulogenic capacity of outgrowing cells as well as the ability of engineered vessels to engage in paracrine signaling and appreciably affect outgrowth.[56,57] Nuclear analysis in our study confirmed deficits in cellular outgrowth density and clustering with RF EGM-2 medium for the + EC_R and − EC_R groups when compared with the growth factor-containing EGM-2 counterparts. Further studies could elucidate specific mechanisms through histological staining of intracellular proteins[36] and analysis of media with protein detection kits to refine our understanding of the angiogenic and preinosculative signaling between engineered vessels and the vascular outgrowth population. In contrast, nonendothelialized channels were similarly unable to stimulate a similar level of outgrowth over the 7 days. Literature showed that channels lacking endothelial monolayers do not inosculate with the host *in vivo*,[15] though they may play a role in facilitating heterocellular ingrowth after migration to the construct[58] and could be pursued in future studies using our platform.

Owing to the short half-life of soluble growth factors both *in vitro* and *in vivo*, controlled release from a biomaterial is a common method of presenting multiple angiogenic stimuli simultaneously[17] or delayed[59] to mimic chemotactic gradients and direct vascularization.[6] We explored the efficacy of growth factor signaling in the absence of endothelialized vessels by loading 10 ng/mL VEGF and bFGF into construct gels cultured in RF EGM-2 and examining the vascular outgrowth response. This concentration was chosen based on our previously published work,[17] and it is low or on par with reported literature on the aortic ring assay (10–50 ng/mL)[32,48,60] and other tissue engineering literature (10–100+ ng/mL).[6,12,59,61]

Increased − EC_{RG} outgrowth as early as day 2 relative to − EC_R kept pace with + EC outgrowth up to day 7, suggesting an equivalently strong and sustained migratory stimulus despite burst release of factor from the constructs[62] and washout from medium exchange on days 3 and 6. Nuclear density and clustering with growth factor release were comparable to the + EC group, and we found no significant differences in − EC_{RG} vimentin-based network formation relative to the negative control or + EC but observed similarly cohesive morphologies to the latter group. These data suggest that local growth factor release is effective in

inducing early and somewhat sustained network-like vascular outgrowth on par with EC-optimized medium containing VEGF and bFGF. Proper combinatorial orchestration of angiogenic factors may effectively instruct chemotactic vascular outgrowth and, in the case of *in vivo* implementation, host inosculation, thus enabling blood flow throughout the bulk of the implant. In translational implementation, there are important tradeoffs to consider in pursuing either localized growth factor release or 3D endothelialized, patterned engineered vessels. Growth factors typically benefit from facile implementation and reduced regulatory burdens but are finite in reserve, whereas patterned, cellularized channels require greater biological engineering to provide an appropriate environment for survival but can persist longer to instruct host vascularization for inosculation. Practical implementation in studies of inosculation necessitate patterned vessels, so future studies could pursue combinatorial implementation of growth factor release from tissues with patterned vessels to provide synergistic benefits in revascularization.

Heterocellular interactions are essential for matrix remodeling and vessel stabilization to vascularize tissues, and histomorphological evaluation of vimentin-positive stromal cells tagged almost all outgrowing cells (verified by nuclear co-staining) and enabled population-level analysis inclusive of the heterocellular population. In addition to the prominent role of endothelial cells (commonly stained using CD-31, IB4) (Supplementary Fig. S6), other cells that support angiogenesis and vascular bed stabilization include pericytes (often labeled by α-SMA, NG-2), smooth muscle cells (α-SMA, SM22), fibroblasts (many possible overlapping markers), and, to a lesser extent, macrophages (CD-45) and dendritic cells (CD-54).[27,32,34] These cell types are present in aortic rings and engage in complex paracrine signaling pathways between endothelial, stromal, and inflammatory cells[63] that potentially provide a more physiologically relevant setting for evaluating angiogenesis, but also additional difficulty in data interpretation.[6,34] Fibroblasts have been shown to be beneficial in supporting the development of functional vasculature,[22] even if only transiently present.[64] VEGF and bFGF additionally act on vascular stromal cell types in a variety of ways (e.g., stimulating smooth muscle migration,[65] proliferation and remodeling in fibroblasts,[66] and inhibiting pericyte vessel stabilization[67]). IGF and EGF are other growth factors present in media compositions and angiogenesis *in vivo* that facilitate endothelial cell growth and tubulogenesis.[36]

We observed qualitatively more cohesive network morphologies in the + EC and − EC_{RG} groups that could be due to greater network formation between endothelial cells and/or recruitment of pericytes or other stromal cells to stabilize new networks and prevent regression. Additional immunohistochemical staining could better elucidate the causes of network differences and identify specific supportive cell types recruited to aortic ring-derived neovessels. Our platform presents a unique foundation to better perturb these complex paracrine signaling interactions in angiogenesis,[63] as they relate to host vascular migration toward inosculation with prepatterned vessels to advance translationally focused tissue engineering.

The versatility of our PDMS mold-based platform allows controlled examination of a broad array of parameters relevant to engineered tissue design, angiogenesis, and complex paracrine and host-implant signaling interactions with aortic rings. Perturbations may include physical cues such as perfusion, distance between and relative orientation of engineered vessels and aortic rings, channel diameter, and gel composition and cellular interactions such as doping in stromal populations into engineered constructs. Further, our platform and the provided analysis tools are adaptable to specific soft tissue engineering applications without the need for significant redesign (e.g., cardiac,[37] skin,[28] or pancreatic[5,68] tissue engineering) by mixing appropriate organ-specific cell types into the collagen-casting mix and seeding in molds with a desired channel geometry, or by placing a prefabricated cellularized scaffold in the construct region.

The platform is also compatible with other prevascularization systems such as self-assembled capillaries[8,22] and patterned cords,[10,11] although our sacrificial templating process provides an additional layer of customization by arranging alginate fibers in different orientations or casting/3D bioprinting alginate in premade templates to create more complex 3D vascular structures.[2,28] This provides additional benefits relative to 2D angiogenesis assays, endothelial cell monolayers seeded on 3D gels that are often utilized in microfluidic/organ-on-a-chip systems, or EC-coated beads embedded in 3D gels.[27] These systems are often highly specialized to focus study on specific mechanisms of vascular biology, such as barrier function[69] and flow dynamics,[25] but can result in limited flexibility with regards to cell–cell interactions and thus signaling, macromorphology,[26] appropriate substrates and stiffnesses,[24] or otherwise be unsuitable for direct comparison to an implantable therapeutic at preclinical scales.[70]

The platform that we designed and used in this study has limitations due to adoption of the aortic ring assay itself. As with any animal-based study, there is an inherent heterogeneity between animals, including factors controlled for in study design (e.g., animal age, location of aortic sections, intima damage during preparation[27]). The larger volume and intermittent exchange of media necessary to accommodate larger engineered tissues in our platform can dilute paracrine signaling from both rings and engineered vessels.[63,71] A broader translational limitation of the platform is its inability to fully predict the host inflammatory response, which plays a key role in stimulating angiogenesis and remodeling during wound healing.[72] Further, longer term (>14 days) assessment of aortic rings is typically not possible as they begin to shift into a regressive state in which sprouts begin to recede and undergo apoptosis. Importantly, there is a lack of perfusion through the aortic rings, which *in vivo* would induce mechanotransductive and mechanochemical signaling to affect endothelial cell outgrowth.[73] However, our platform allows for perfusion of engineered vessels, providing additional versatility that may elucidate flow-driven mechanisms of pro-angiogenic vascular signaling between host and implanted tissue.

Conclusions

In summary, our novel platform uses the aortic ring assay in co-culture with engineered constructs in a complex, defined environment to investigate preinosculative vascular cell outgrowth with greater ability to control environmental

signals as compared with *in vivo* studies. Using robust, open-source quantitative tools, we report for the first time that both endothelial cell-lined vessels and local growth factor release comparably promote early chemotaxis from surrogate host heterocellular host vascular populations, which is less pronounced with nonendothelialized channels, media lacking key angiogenic growth factors, or both. Our platform provides a flexible foundation for perturbing effectors of preinosculative heterotypic vascular outgrowth and evaluating host-instructive vascularization cues from engineered therapeutics for regenerative medicine applications.

Authors' Contributions

All authors contributed significantly to this article.

Acknowledgments

The authors would like to acknowledge Geoffrey Williams from the Brown University Leduc Bioimaging Facility for training and use of the confocal microscope; Christopher Bull with the Brown Design Workshop for laser cutter training, support, and access; and Elaina Atherton and Dr. Aastha Kapoor for assistance in developing histological staining procedures.

Disclosure Statement

All authors have no conflicts of interest to disclose.

Funding Information

This work was supported by funding from NIH R01 HL135091 (to K.L.K.C).

Supplementary Material

Supplementary Figure S1
Supplementary Figure S2
Supplementary Figure S3
Supplementary Figure S4
Supplementary Figure S5
Supplementary Figure S6
Supplementary Figure S7
Supplementary Figure S8
Supplementary Movie S1

References

1. Radisic, M., Malda, J., Epping, E., Geng, W., Langer, R., and Vunjak-Novakovic, G. Oxygen gradients correlate with cell density and cell viability in engineered cardiac tissue. Biotechnol Bioeng **93,** 332, 2006.
2. Vollert, I., Seiffert, M., Bachmair, J., *et al.* In vitro perfusion of engineered heart tissue through endothelialized channels. Tissue Eng Part A **20,** 854, 2014.
3. Radisic, M., Yang, L., Boublik, J., *et al*. Medium perfusion enables engineering of compact and contractile cardiac tissue. Am J Physiol Circ Physiol **286,** H507, 2004.
4. Laflamme, M.A., and Murry, C.E. Regenerating the heart. Nat Biotechnol **23,** 845, 2005.
5. Salg, G.A., Giese, N.A., Schenk, M., *et al.* The emerging field of pancreatic tissue engineering: a systematic review and evidence map of scaffold materials and scaffolding techniques for insulin-secreting cells. J Tissue Eng **10,** 1, 2019.
6. Kant, R.J., and Coulombe, K.L.K. Integrated approaches to spatiotemporally directing angiogenesis in host and engineered tissues. Acta Biomater **69,** 42, 2018.
7. Miller, J.S., Stevens, K.R., Yang, M.T.M.T., *et al.* Rapid casting of patterned vascular networks for perfusable engineered three-dimensional tissues. Nat Mater **11,** 768, 2012.
8. Schaefer, J.A., Guzman, P.A., Riemenschneider, S.B., Kamp, T.J., and Tranquillo, R.T. A cardiac patch from aligned microvessel and cardiomyocyte patches. J Tissue Eng Regen Med **12,** 546, 2018.
9. Redd, M.A., Zeinstra, N., Qin, W., *et al.* Patterned human microvascular grafts enable rapid vascularization and increase perfusion in infarcted rat hearts. Nat Commun **10,** 1, 2019.
10. Brady, E.L., Kirby, M.A., Olszewski, E., *et al.* Guided vascularization in the rat heart leads to transient vessel patterning. APL Bioeng **4,** 016105, 2020.
11. Baranski, J.D., Chaturvedi, R.R., Stevens, K.R., *et al.* Geometric control of vascular networks to enhance engineered tissue integration and function. Proc Natl Acad Sci U S A **110,** 7586, 2013.
12. Wu, Q., Li, Y., Wang, Y., *et al.* The effect of heparinized decellularized scaffolds on angiogenic capability. J Biomed Mater Res Part A **104,** 3021, 2016.
13. Abaci, H.E., Guo, Z., Coffman, A., *et al*. Human skin constructs with spatially controlled vasculature using primary and iPSC-derived endothelial cells. Adv Healthc Mater **5,** 1800, 2016.
14. Noor, N., Shapira, A., Edri, R., Gal, I., Wertheim, L., and Dvir, T. 3D printing of personalized thick and perfusable cardiac patches and hearts. Adv Sci **6,** 1900344, 2019.
15. Mirabella, T., MacArthur, J.W., Cheng, D., *et al*. 3D-printed vascular networks direct therapeutic angiogenesis in ischaemia. Nat Biomed Eng **1,** 0083, 2017.
16. Song, M., Jang, H., Lee, J., *et al*. Regeneration of chronic myocardial infarction by injectable hydrogels containing stem cell homing factor SDF-1 and angiogenic peptide Ac-SDKP. Biomaterials **35,** 2436, 2014.
17. Munarin, F., Kant, R.J., Rupert, C.E., Khoo, A., and Coulombe, K.L.K. Engineered human myocardium with local release of angiogenic proteins improves vascularization and cardiac function in injured rat hearts. Biomaterials **251,** 120033, 2020.
18. Morrissette-McAlmon, J., Ginn, B., Somers, S., *et al.* Biomimetic model of contractile cardiac tissue with endothelial networks stabilized by adipose-derived stromal/stem cells. Sci Rep **10,** 8387, 2020.
19. Kim, J.J., Hou, L., and Huang, N.F. Vascularization of three-dimensional engineered tissues for regenerative medicine applications. Acta Biomater **41,** 17, 2016.
20. Laschke, M.W., Vollmar, B., and Menger, M.D. Inosculation: connecting the life-sustaining pipelines. Tissue Eng Part B Rev **15,** 455, 2009.
21. Utzinger, U., Baggett, B., Weiss, J.A., Hoying, J.B., and Edgar, L.T. Large-scale time series microscopy of neovessel growth during angiogenesis. Angiogenesis **18,** 219, 2015.
22. Chen, X., Aledia, A.S., Popson, S.A., Him, L., Hughes, C.C.W., and George, S.C. Rapid anastomosis of endothelial progenitor cell–derived vessels with host vasculature is promoted by a high density of cotransplanted fibroblasts. Tissue Eng Part A **16,** 585, 2010.

23. White, S.M., Pittman, C.R., Hingorani, R., *et al.* Implanted cell-dense prevascularized tissues develop functional vasculature that supports reoxygenation after thrombosis. Tissue Eng Part A **20,** 2316, 2014.
24. Wang, X., Phan, D.T.T., Sobrino, A., George, S.C., Hughes, C.C.W., and Lee, A.P. Engineering anastomosis between living capillary networks and endothelial cell-lined microfluidic channels. Lab Chip **16,** 282, 2016.
25. Kim, S., Chung, M., Ahn, J., Lee, S., and Jeon, N.L. Interstitial flow regulates the angiogenic response and phenotype of endothelial cells in a 3D culture model. Lab Chip **16,** 4189, 2016.
26. de Graaf, M.N.S., Cochrane, A., van den Hil, F.E., *et al.* Scalable microphysiological system to model three-dimensional blood vessels. APL Bioeng **3,** 026105, 2019.
27. Nowak-Sliwinska, P., Alitalo, K., Allen, E., *et al.* Consensus guidelines for the use and interpretation of angiogenesis assays. Angiogenesis **21,** 425, 2018.
28. Debbi, L., Zohar, B., Shandalov, Y., and Levenberg, S. Integrating engineered macro vessels with self-assembled capillaries in 3D implantable tissue for promoting vascular integration in-vivo. BioRxiv 2020 [Epub ahead of print]; DOI: 10.1101/2020.07.07.190900.
29. Nowak-Sliwinska, P., Segura, T., Iruela-Arispe, M.L., and Angeles, L. The chicken chorioallantoic membrane model in biology, medicine and bioengineering. Angiogenesis **17,** 779, 2014.
30. Rezzola, S., Belleri, M., Gariano, G., *et al*. In vitro and ex vivo retina angiogenesis assays. Angiogenesis **17,** 429, 2014.
31. Stiffey-Wilusz, J., Boice, J.A., Ronan, J., Fletcher, A.M., and Anderson, M.S. An ex vivo angiogenesis assay utilizing commercial porcine carotid artery: modification of the rat aortic ring assay. Angiogenesis **4,** 3, 2001.
32. Nicosia, R.F. The aortic ring model of angiogenesis: a quarter century of search and discovery. J Cell Mol Med **13,** 4113, 2009.
33. Masson, V., Devy, L., Grignet-Debrus, C., *et al.* Mouse aortic ring assay: a new approach of the molecular genetics of angiogenesis. Biol Proced Online **4,** 24, 2002.
34. Chiaverina, G., di Blasio, L., Monica, V., *et al.* Dynamic interplay between pericytes and endothelial cells during sprouting angiogenesis. Cells **8,** 1109, 2019.
35. Rawal, S., Munasinghe, P.E., Shindikar, A., *et al.* Down-regulation of proangiogenic microRNA-126 and microRNA-132 are early modulators of diabetic cardiac microangiopathy. Cardiovasc Res **113,** 90, 2017.
36. Kapoor, A., Chen, C.G., and Iozzo, R.V. A simplified aortic ring assay: a useful ex vivo method to assess biochemical and functional parameters of angiogenesis. Matrix Biol Plus **6,** 100025, 2020.
37. Munarin, F., Kaiser, N.J., Kim, T.Y., Choi, B.-R., and Coulombe, K.L.K. Laser-etched designs for molding hydrogel-based engineered tissues. Tissue Eng Part C Methods **23,** 311, 2017.
38. Go, R.S., and Owen, W.G. The rat aortic ring assay for in vitro study of angiogenesis. Methods Mol Med **85,** 59, 2003.
39. Dave, J.M., and Bayless, K.J. Vimentin as an integral regulator of cell adhesion and endothelial sprouting. Microcirculation **21,** 333, 2014.
40. Stapor, P.C., Sweat, R.S., Dashti, D.C., Betancourt, A.M., and Murfee, W.L. Pericyte dynamics during angiogenesis: new insights from new identities. J Vasc Res **51,** 163, 2014.
41. Gabbiani, G., Schmidt, E., Wintert, S., *et al.* Vascular smooth muscle cells differ from other smooth muscle cells: predominance of vimentin filaments and a specific a-type actin. Proc Natl Acad Sci U S A **78,** 298, 1981.
42. Avolio, E., Alvino, V. V., Ghorbel, M.T., and Campagnolo, P. Perivascular cells and tissue engineering: current applications and untapped potential. Pharmacol Ther **171,** 83, 2017.
43. Moya, M.L., Hsu, Y.-H., Lee, A.P., Hughes, C.C.W., and George, S.C. In vitro perfused human capillary networks. Tissue Eng Part C Methods **19,** 730, 2013.
44. Mian, R., Morrison, W.A, Hurley, J.V, *et al*. Formation of new tissue from an arteriovenous loop in the absence of added extracellular matrix. Tissue Eng **6,** 595, 2000.
45. Lehr, H.A., Leunig, M., Menger, M.D., Nolte, D., and Messmer, K. Dorsal skinfold chamber technique for intravital microscopy in nude mice. Am J Pathol **143,** 1055, 1993.
46. White, S.M., Hingorani, R., Arora, R.P.S., Hughes, C.C.W., George, S.C., and Choi, B. Longitudinal in vivo imaging to assess blood flow and oxygenation in implantable engineered tissues. Tissue Eng Part C Methods **18,** 697, 2012.
47. Nicosia, R.F., Zhu, W.-H., Fogel, E., Howson, K.M., and Aplin, A.C. A new ex vivo model to study venous angiogenesis and arterio-venous anastomosis formation. J Vasc Res **42,** 111, 2005.
48. Aplin, A.C., and Nicosia, R.F. The plaque-aortic ring assay: a new method to study human atherosclerosis-induced angiogenesis. Angiogenesis **22,** 421, 2019.
49. Lee, K.Y., and Mooney, D.J. Alginate: properties and biomedical applications. Prog Polym Sci **37,** 106, 2012.
50. Watson, E.C., Grant, Z.L., and Coultas, L. Endothelial cell apoptosis in angiogenesis and vessel regression. Cell Mol Life Sci **74,** 4387, 2017.
51. Goodwin, A.M. In vitro assays of angiogenesis for assessment of angiogenic and anti-angiogenic agents. Microvasc Res **74,** 172, 2007.
52. Tung, J.J., Tattersall, I.W., and Kitajewski, J. Tips, stalks, tubes: notch-mediated cell fate determination and mechanisms of tubulogenesis during angiogenesis. Cold Spring Harb Perspect Med **2,** a006601, 2012.
53. Phng, L.K., Potente, M., Leslie, J.D., *et al.* Nrarp coordinates endothelial Notch and Wnt signaling to control vessel density in angiogenesis. Dev Cell **16,** 70, 2009.
54. Cross, M.J., and Claesson-Welsh, L. FGF and VEGF function in angiogenesis: signalling pathways, biological responses and therapeutic inhibition. Trends Pharmacol Sci **22,** 201, 2001.
55. Iularo, M., Scatena, M., Zhu, W.H., Fogel, E., Wieting, S.L., and Nicosia, R.F. Rat aorta-derived mural precursor cell express the Tie2 receptor and respond directly to stimulation by angiopoietins. J Cell Sci **116,** 3635, 2003.
56. Leopold, B., Strutz, J., Weiß, E., *et al.* Outgrowth, proliferation, viability, angiogenesis and phenotype of primary human endothelial cells in different purchasable endothelial culture media: feed wisely. Histochem Cell Biol **152,** 377, 2019.
57. Lafleur, M.A., Handsley, M.M., Knäuper, V., Murphy, G., and Edwards, D.R. Endothelial tubulogenesis within fibrin gels specifically requires the activity of membrane-type-matrix metalloproteinases (MT-MMPs). J Cell Sci **1,** 3427, 2002.
58. Tang, F., Manz, X.D., Bongers, A., *et al.* Microchannels are an architectural cue that promotes integration and vascularization of silk biomaterials in vivo. ACS Biomater Sci Eng **6,** 1476, 2020.

59. Brudno, Y., Ennett-Shepard, A.B., Chen, R.R., Aizenberg, M., and Mooney, D.J. Enhancing microvascular formation and vessel maturation through temporal control over multiple pro-angiogenic and pro-maturation factors. Biomaterials **34,** 9201, 2013.
60. Baker, M., Robinson, S.D., Lechertier, T., *et al.* Use of the mouse aortic ring assay to study angiogenesis. Nat Protoc **7,** 89, 2012.
61. Izadifar, M., Kelly, M.E., and Chen, X. Regulation of sequential release of growth factors using bilayer polymeric nanoparticles for cardiac tissue engineering. Nanomedicine **11,** 3237, 2016.
62. Tabata, Y., Miyao, M., Ozeki, M., and Ikada, Y. Controlled release of vascular endothelial growth factor by use of collagen hydrogels. J Biomater Sci Polym Ed **11,** 915, 2000.
63. Nicosia, R.F., Zorzi, P., Ligresti, G., Morishita, A., and Aplin, A.C. Paracrine regulation of angiogenesis by different cell types in the aorta ring model. Int J Dev Biol **55,** 447, 2011.
64. Song, H.G., Lammers, A., Sundaram, S., *et al.* Transient support from fibroblasts is sufficient to drive functional vascularization in engineered tissues. Adv Funct Mater **30,** 2003777, 2020.
65. Grosskreutz, C.L., Anand-Apte, B., Dupláa, C., *et al*. Vascular endothelial growth factor-induced migration of vascular smooth muscle cells in vitro. Microvasc Res **58,** 128, 1999.
66. Makino, T., Jinnin, M., Muchemwa, F.C.C., *et al.* Basic fibroblast growth factor stimulates the proliferation of human dermal fibroblasts via the ERK1/2 and JNK pathways. Br J Dermatol **162,** 717, 2009.
67. Greenberg, J.I., Shields, D.J., Barillas, S.G., *et al.* A role for VEGF as a negative regulator of pericyte function and vessel maturation. Nature **456,** 809, 2008.
68. Kim, J., Shim, I.K., Hwang, D.G., *et al.* 3D cell printing of islet-laden pancreatic tissue-derived extracellular matrix bioink constructs for enhancing pancreatic functions. J Mater Chem B **7,** 1773, 2019.
69. Polacheck, W.J., Kutys, M.L., Yang, J., *et al.* A non-canonical Notch complex regulates adherens junctions and vascular barrier function. Nature **552,** 258, 2017.
70. Shin, Y., Jeon, J.S., Han, S., *et al.* In vitro 3D collective sprouting angiogenesis under orchestrated ANG-1 and VEGF gradients. Lab Chip **11,** 2175, 2011.
71. Nicosia, R.F., Lin, Y.J., Hazelton, D., and Qian, X.H. Endogenous regulation of angiogenesis in the rat aorta model: role of vascular endothelial growth factor. Am J Pathol **151,** 1379, 1997.
72. Barrientos, S., Stojadinovic, O., Golinko, M.S., Brem, H., and Tomic-Canic, M. Growth factors and cytokines in wound healing. Wound Repair Regen **16,** 585, 2008.
73. Lamalice, L., Le Boeuf, F., and Huot, J. Endothelial cell migration during angiogenesis. Circ Res **100,** 782, 2007.

Address correspondence to:
Kareen L.K. Coulombe, PhD
Center for Biomedical Engineering
School of Engineering
Brown University
184 Hope St.
Providence, RI 02912
USA

E-mail: kareen_coulombe@brown.edu

Received: September 8, 2020
Accepted: January 11, 2021
Online Publication Date: March 2, 2021